

Schottky MSM junctions for carrier depletion in silicon photonic crystal microcavities

Laurent-Daniel Haret,¹ Xavier Checoury,^{1,*} Fabien Bayle,¹ Nicolas Cazier,¹ Philippe Boucaud,¹ Sylvain Combrié,² and Alfredo de Rossi²

¹ Institut d'Electronique Fondamentale. Bâtiment 220, Univ. Paris Sud
CNRS UMR 8622 F-91405 Orsay France

² Thales Research and Technology. 1 avenue Augustin Fresnel 91707 Palaiseau France

*xavier.checoury@ief.u-psud.fr

Abstract: Collection of free carriers is a key issue in silicon photonics devices. We show that a lateral metal-semiconductor-metal Schottky junction is an efficient and simple way of dealing with that issue in a photonic crystal microcavity. Using a simple electrode design, and taking into account the optical mode profile, the resulting carrier distribution in the structure is calculated. We show that the corresponding effective free carrier lifetime can be reduced by 50 times when the bias is tuned. This allows one to maintain a high cavity quality factor under strong optical injection. In the fabricated structures, carrier depletion is correlated with transmission spectra and directly visualized by Electron Beam Induced Current pictures. These measurements demonstrate the validity of this carrier extraction principle. The design can still be optimized in order to obtain full carrier depletion at a smaller energy cost.

© 2013 Optical Society of America

OCIS codes: (230.5298) Photonic crystals; (230.2090) Electro-optical devices; (140.3948) Microcavity devices.

References and links

1. B. Jalali and S. Fathpour, "Silicon photonics," *J. Lightw. Technol.* **24**, 4600–4615 (2006).
2. M. El Kurdi, P. Boucaud, S. Sauvage, G. Fishman, O. Kermarrec, Y. Campidelli, D. Bensahel, G. Saint-Girons, I. Sagnes, and G. Patriarche, "Silicon-on-insulator waveguide photodetector with Ge/Si self-assembled islands," *J. Appl. Phys.* **92**, 1858–1861 (2002).
3. J. K. Doyle, P. E. Jessop, and A. P. Knights, "Silicon photonic resonator-enhanced defect-mediated photodiode for sub-bandgap detection," *Opt. Express* **18**, 14671–14678 (2010).
4. H. C. Nguyen, Y. Sakai, M. Shinkawa, N. Ishikura, and T. Baba, "Photonic crystal silicon optical modulators: Carrier-injection and depletion at 10 Gb/s," *IEEE J. Quantum Electron.* **48**, 210–220 (2012).
5. G. Reed, G. Mashanovich, F. Y. Gardes, and D. J. Thomson, "Silicon optical modulators," *Nat. Photon.* **4**, 518–526 (2010).
6. L. Liu, R. Kumar, K. Huybrechts, T. Spuesens, G. Roelkens, E.-J. Geluk, T. de Vries, P. Regreny, D. Van Thourhout, R. Baets, and G. Morthier, "An ultra-small, low-power, all-optical flip-flop memory on a silicon chip," *Nat. Photon.* **4**, 182–187 (2010).
7. T. Tanabe, M. Notomi, S. Mitsugi, A. Shinya, and E. Kuramochi, "Fast bistable all-optical switch and memory on a silicon photonic crystal on-chip," *Opt. Lett.* **30**, 2575–2577 (2005).
8. M. Hill, H. Dorren, T. de Vries, X. Leijtens, J. Besten, B. Smallbrugge, Y.-S. Oei, H. Binsma, G.-D. Khoe, and M. Smit, "A fast low-power optical memory based on coupled micro-ring lasers," *Nature* **432**, 206–209 (2004).
9. Z. Han, X. Checoury, D. Néel, S. David, M. El Kurdi, and P. Boucaud, "Optimized design for 2×10^6 ultra-high Q silicon photonic crystal cavities," *Opt. Comm.* **283**, 4387–4391 (2010).

10. H. Rong, S. Xu, Y.-H. Kuo, V. Sih, O. Cohen, O. Raday, and M. Paniccia, "Low-threshold continuous-wave Raman silicon laser," *Nat. Photon.* **1**, 232–237 (2007).
11. X. Checoury, Z. Han, and P. Boucaud, "Stimulated Raman scattering in silicon photonic crystal waveguides under continuous excitation," *Phys. Rev. B* **82**, 041308 (2010).
12. C. Monat, M. Ebnali-Heidari, C. Grillet, B. Corcoran, B. J. Eggleton, T. P. White, L. O'Faolain, J. Li, and T. F. Krauss, "Four-wave mixing in slow light engineered silicon photonic crystal waveguides," *Opt. Express* **18**, 22915–22927 (2010).
13. T. J. Johnson and O. Painter, "Passive modification of free carrier lifetime in high-Q silicon-on-insulator optics," 2009 Conf. On Lasers and Electro-optics and Quantum Electronics and Laser Science Conf. (cleo/qels 2009), Vols 1-5 pp. 72–73 (2009).
14. A. Berrier, M. Mulot, G. Malm, M. Ostling, and S. Anand, "Carrier transport through a dry-etched InP-based two-dimensional photonic crystal," *J. Appl. Phys.* **101**, 123101 (2007).
15. P. Cardile, G. Franzo, R. L. Savio, M. Galli, T. F. Krauss, F. Priolo, and L. O. Faolain, "Electrical conduction and optical properties of doped silicon-on-insulator photonic crystals," *Appl. Phys. Lett.* **98**, 203506 (2011).
16. B. Ellis, T. Sarmiento, M. Mayer, B. Zhang, J. Harris, E. Haller, and J. Vuckovic, "Electrically pumped photonic crystal nanocavity light sources using a laterally doped p-i-n junction," *Appl. Phys. Lett.* **96**, 181103 (2010).
17. J. Petykiewicz, G. Shambat, B. Ellis, and J. Vuckovic, "Electrical properties of GaAs photonic crystal cavity lateral p-i-n diodes," *Appl. Phys. Lett.* **101**, 011104 (2012).
18. T. Tanabe, K. Nishiguchi, E. Kuramochi, and M. Notomi, "Low power and fast electro-optic silicon modulator with lateral p-i-n embedded photonic crystal nanocavity," *Opt. Express* **17**, 22505–22513 (2009).
19. L.-D. Haret, X. Checoury, Z. Han, P. Boucaud, S. Combrié, and A. De Rossi, "All-silicon photonic crystal photodiode on silicon-on-insulator at telecom wavelength," *Opt. Express* **18**, 23965–23972 (2010).
20. T. Tanabe, H. Sumikura, H. Taniyama, A. Shinya, and M. Notomi, "All-silicon sub-Gb/s telecom detector with low dark current and high quantum efficiency on chip," *Appl. Phys. Lett.* **96**, 101103 (2010).
21. R. Hayakawa, N. Ishikura, H. C. Nguyen, and T. Baba, "Two-photon-absorption photodiodes in Si photonic-crystal slow-light waveguides," *Appl. Phys. Lett.* **102**, 031114 (2013).
22. R. Soref and B. Bennett, "Electrooptical effects in silicon," *IEEE J. Quantum Electron.* **23**, 123–129 (1987).
23. Q. Lin, O. J. Painter, and G. P. Agrawal, "Nonlinear optical phenomena in silicon waveguides: Modeling and applications," *Opt. Express* **15**, 16604–16644 (2007).
24. E. Kuramochi, M. Notomi, S. Mitsugi, A. Shinya, T. Tanabe, and T. Watanabe, "Ultra-high-Q photonic crystal nanocavities realized by the local width modulation of a line defect," *Appl. Phys. Lett.* **88**, 041112 (2006).
25. S. Selberherr, *Analysis and Simulation of Semiconductor Devices* (Springer-Verlag, 1984).
26. C. Canali, C. Jacoboni, F. Nava, G. Ottaviani, and A. Alberigi-Quaranta, "Electron drift velocity in silicon," *Phys. Rev. B* **12**, 2265–2284 (1975).
27. S. M. Sze and K. K. Ng, *Physics of Semiconductor Devices* (Wiley-Blackwell, 2006 (3rd edition)).
28. S. Sze, D. C. Jr., and A. Loya, "Current transport in metal-semiconductor-metal (MSM) structures," *Solid-State Electron.* **14**, 1209 – 1218 (1971).
29. T. E. Everhart, O. C. Welles, and C. W. Oatley, "Factors affecting contrast and resolution in the scanning electron microscope," *J. Electron. Control* **7**, 97–111 (1959).
30. T. E. Everhart, O. C. Wells, and R. K. Matta, "A novel method of semiconductor device measurements," *Proc. IEEE* **52**, 1642–1647 (1964).
31. K. O. Leedy, "A bibliography on electron beam induced current analysis of semiconductor devices," *Solid-State Tech.* **20**, 45–48 (1977).
32. W. A. Wohlmuth, M. Arafa, A. Mahajan, P. Fay, and I. Adesida, "InGaAs metal-semiconductor-metal photodetectors with engineered Schottky barrier heights," *Appl. Phys. Lett.* **69**, 3578–3580 (1996).
33. C. O. Chui, A. K. Okyay, and K. C. Saraswat, "Effective dark current suppression with asymmetric MSM photodetectors in group IV semiconductors," *IEEE Photon. Technol. Lett.* **15**, 1585–1587 (2003).

1. Introduction

Silicon photonics is a very promising platform for on-chip integration of electronics with all-optical interconnects [1]. Over the last years, all-silicon micron-sized Complementary Metal Oxide Semiconductor (CMOS) compatible devices, including detectors [2, 3], modulators at telecom wavelength [4, 5] and all-optical logical memories [6, 7] have been demonstrated. The most compact components rely on a built-in optical resonator with a high quality factor, most currently a microring [8] or a 2D photonic crystal cavity [9]. In this article, we discuss a technique to control the carrier concentration in photonic crystals (PhCs). In these devices, the free carrier density is a crucial parameter, because it determines the strength of the free carrier absorption (FCA) and free carrier dispersion (FCD) effects. In photonic crystal slow light

waveguides or in PhC microcavities, free carriers generated by two-photon absorption lead to the strong increase of propagation losses or to the collapse of the quality factor at high optical power. This is considered as a serious limitation to achieve ultra-compact devices thanks to PhCs such as a silicon Raman laser [10, 11] or four-wave-mixing based wavelength converters [12].

There are two general methods to get rid of free carriers in a photonic crystal structure: increasing the surface recombination velocity by a chemical treatment [13], or sweeping the carriers away by applying an electric field. With the first method, however, it is impossible to tune the effect on demand. The second method is challenging as it requires to integrate an electrical junction nearby the photonic crystal resonator. If ohmic contacts [14, 15] or a *p-i-n* junction [16–18] are chosen, several more steps are needed in the fabrication process in order to implant locally the silicon under the contacts (in the ohmic junction case) or to form the *p* and *n* regions. Further complications may arise concerning the junction impact on the overall mode absorption, and the change in the material conductivity caused by the geometry and the surface states of the chemically etched photonic crystal.

If a metal-semiconductor-metal (MSM) lateral Schottky junction is used instead, there is no more need for any implantation. The MSM platform is a mature technology for high-speed optoelectronics components. As compared to a *p-i-n* junction where the diode structure creates a non-negligible capacitance, for a similar size of the intrinsic area and an optimized design, it is possible to get a much lower capacitance and thus a faster response in a MSM device. The major drawback of MSM technology can be the higher reverse current. However, if needed (depending on the application) it can be reduced by a careful choice of the metal contact. As for the impact of the metal absorption on the optical resonator, we previously showed that losses can be dealt with by a careful design [19] at the expense of a larger separation of the electrodes [20, 21]. Thus the remaining issue is to check that carrier collection in a MSM photonic crystal junction can be effective and very fast. In this paper, we will focus on that aspect. After a quantitative description of the impact of free carrier lifetime on the quality factor in a silicon microcavity, a 2D Technology Computer Aided Design (TCAD) calculation of carrier distribution and collection efficiency is performed. Its results show that effective and fast carrier collection is ensured when the depletion region around one of the polarized electrodes overlaps most of the mode volume. Consequently, high quality factor can be maintained even under strong optical pumping. Electron-Beam Induced Current (EBIC) images of the depletion region then confirm the simulation results and the validity of our design. In the last section, we discuss how the device can be improved in order to reduce the operating energy cost.

2. Maintaining a high quality factor in a PhC microcavity

The reason for trying to get rid of free carriers in a silicon microcavity is easily explained with an analytical model of non-linear losses in the structure. The losses include two-photon absorption (TPA), and FCA. At telecom wavelengths, free carriers are introduced in the structure by three mechanisms: residual impurities, two-photon absorption, and the residual linear absorption. The losses induced by carriers introduced by residual impurities are linear losses and are already included in the intrinsic quality factor. Thus, at the cavity resonance, the field amplitude A in the cavity follows the following equation:

$$\frac{dA}{dt} = - \left[\frac{\omega_0}{2Q} + \frac{\beta_{\text{TPA}}}{2V_{\text{TPA}}} \left(\frac{c}{n_{\text{Si}}} \right)^2 |A|^2 + \frac{1}{2} \left(\frac{c}{n_{\text{Si}}} \right) \sigma_{\text{FCA}} n_{\text{ph}}^{\text{eff}} \right] A + \left(\frac{\omega_0 \sqrt{\text{Tr}_0}}{2Q} P_{\text{in}} \right)^{1/2} \quad (1)$$

where P_{in} is the input power, Tr_0 is the low power cavity transmission at resonance, Q is the quality factor in the linear optical regime. $n_{\text{ph}}^{\text{eff}}$ is the effective density of photogenerated carriers and will be defined later on. The other coefficients are constant parameters:

$\beta_{\text{TPA}} = 8 \times 10^{-12} \text{ m} \cdot \text{W}^{-1}$ is the TPA coefficient, $\sigma_{\text{FCA}} = 14.5 \times 10^{-18} \text{ cm}^2$ the free carrier absorption cross-section at 1550 nm [22], and $n_{\text{Si}} = 3.45$ the refractive index of silicon. In steady state, the effective quality factor of the cavity is defined as $Q_{\text{eff}} = \frac{\omega_0}{2\sqrt{\text{Tr}_0}} \frac{|A|^2}{P_{\text{in}}}$. From Eq. (1), we derive

$$Q_{\text{eff}}^{-1} = Q^{-1} + \left(\frac{\omega_0 V_{\text{TPA}} n_{\text{Si}}^2}{\beta_{\text{TPA}} c^2 |A|^2} \right)^{-1} + \left(\frac{\omega_0 n_{\text{Si}}}{c \sigma_{\text{FCA}} n_{\text{ph}}^{\text{eff}}} \right)^{-1} \quad (2)$$

Photogenerated carriers are created locally at a generation rate g that depends on the local absorption, that is to say on the local electric field. The effective photogenerated carrier density $n_{\text{ph}}^{\text{eff}}$ is a mean value that takes into account the overlap between the optical mode and carrier distribution profile, which is the significant quantity for representing total FCA [23]:

$$n_{\text{ph}}^{\text{eff}} := \frac{\iiint_{\text{Si}} n_{\text{ph}}(\mathbf{r}) n_{\text{Si}}^2 |\mathbf{E}|^2(\mathbf{r}) d^3 r}{\iiint_{\mathcal{V}} n_0^2(\mathbf{r}) |\mathbf{E}|^2(\mathbf{r}) d^3 r} \quad (3)$$

where $n_0(\mathbf{r}) = 1$ in the air and $n_0(\mathbf{r}) = n_{\text{Si}}$ in silicon. By integrating the diffusion equation for carriers in space, as in [23] one derives $n_{\text{ph}}^{\text{eff}} = \tau_{fc} g^{\text{eff}}$, where g^{eff} is an effective generation rate. τ_{fc} is the carrier lifetime in the cavity. It includes disappearance of carriers by recombination and by diffusion out of the cavity. This parameter is now the only unknown of our model.

The evolution of Q_{eff} as a function of the input power for different effective carrier lifetimes is shown in Fig. 1. The resonator considered here is the typical width-modulated W1 microcavity [24] frequently used in photonic crystal devices. For $Q_0 = 50,000$, there is an input power range where TPA loss is still negligible, but FCA-related loss is already significant: in Fig. 1, this corresponds to $100 \mu\text{W} < P_{\text{in}} < 800 \mu\text{W}$. Hence, a reduction of carrier lifetime would allow to maintain the quality factor, in that input power range. When the input power is large, there is a decrease of the effective quality factor due to TPA along with a decrease due to FCA. The latter is the main contribution when the free-carrier lifetime is large. Thus, decreasing the free carrier lifetime can provide a significant improvement of the effective quality factor. The effective lifetimes reported in silicon microcavities range between 0.1 and 1 ns. 0.1 ns is obtained with a chemical treatment [13]. This is not short enough to eliminate completely FCA in the interesting power range: it would be useful to have the effective lifetime go down 10 ps. This may be possible with a MSM junction.

3. Reduction of effective carrier lifetime with a MSM junction

The following step is to estimate the reduction of free carrier lifetime that can be obtained when polarizing a lateral MSM junction around the resonator. This implies the knowledge of the free carrier distribution of the illuminated photonic crystal. In that purpose, a 2D Technology Computer Aided Design (TCAD) simulation was performed using the ATLAS software which solves the drift-diffusion, carrier generation and Poisson equations by a finite-element method algorithm. The investigated structure is a triangular lattice air hole photonic crystal with a missing hole row in the ΓK direction (namely a W1 waveguide) and two lateral Schottky electrodes that are symmetrical with respect to the waveguide center. The simulation domain is limited to the active region represented in Fig. 2(a). The lattice parameter a is 400 nm and the electrode spacing is 3 μm . The air holes were approximated as 20 side polygons and the smallest mesh size was 20 nm. The Schottky electrodes were modeled with a double boundary

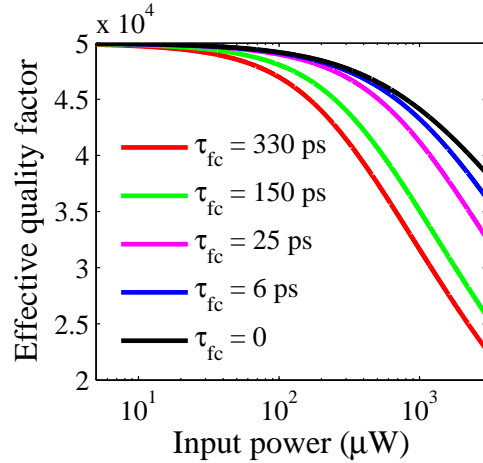


Fig. 1. Dependence of the effective quality factor on the input power for different effective carrier lifetimes in a width-modulated W1 waveguide photonic crystal cavity. The decrease of the quality factor is due to the cumulated effect of two-photon absorption, and free-carrier absorption (FCA). The latter effect is dominant as soon as the free carrier lifetime τ_{fc} is larger than 50 ps.

condition on the surface potential ϕ_S and on the outgoing current flux:

$$\phi_S = V_{\text{appl}} - \frac{E_{Bn}}{q} + (E_C - E_F) \quad (4)$$

$$J_{n,p}^{\perp} = \frac{A_{n,p}^{**} T^2}{q N_C} (n_{e,h} - n_{e,h}^{\text{eq}}) \quad (5)$$

where E_{Bn} is the potential barrier, E_C and E_F are the bottom of the conduction band and the Fermi level, $A_n^{**} = 110 \text{ A} \cdot \text{cm}^{-2} \cdot \text{K}^{-2}$ and $A_p^{**} = 30 \text{ A} \cdot \text{cm}^{-2} \cdot \text{K}^{-2}$ are the tabulated effective Richardson constants for electrons and for holes in silicon, $n_{e,h}^{\text{eq}}$ are the equivalent carrier densities when the surface recombination velocity is infinite, and N_C is the density of states in the conduction band. The model includes Auger and Shockley-Read-Hall (SRH) recombination mechanisms, Selberherr's model for impact ionization in silicon [25] and the mobility is dependent on the strength of the electric field, so that the carrier saturation velocity is $1 \times 10^7 \text{ cm} \cdot \text{s}^{-1}$ [26]. The impurity donor concentration parameter N_D is $4 \times 10^{15} \text{ cm}^{-3}$ and the bulk recombination SRH time is $0.5 \mu\text{s}$.

The simulation results when there is no illumination ($g = 0$) give some insight on the carrier collection mechanisms [Fig. 2(b)]. The key parameter for interpretation is the depletion width W , given by the following equation ([27]):

$$W = \sqrt{\frac{2\epsilon_0\epsilon_{\text{Si}}}{q^2 N_D} \left(E_{Bn} - k_B T \left(\ln \frac{N_C}{N_D} + 1 \right) - qV_{\text{appl}} \right)} \quad (6)$$

where V_{appl} is the externally applied potential, $\epsilon_{\text{Si}} = 11.9$ the dielectric constant of silicon, and N_C the effective density of states in the conduction band. When $V_{\text{appl}} = 0$, W is smaller than the electrode spacing. At small bias, only the diffusion electrons can contribute to the dark current, because holes recombine in the region that is not depleted. However, as soon as the depletion regions around each electrode reach each other, the drift of holes becomes the main contribution. This accounts for the first discontinuity around 30 V in the $I(V)$ curve,

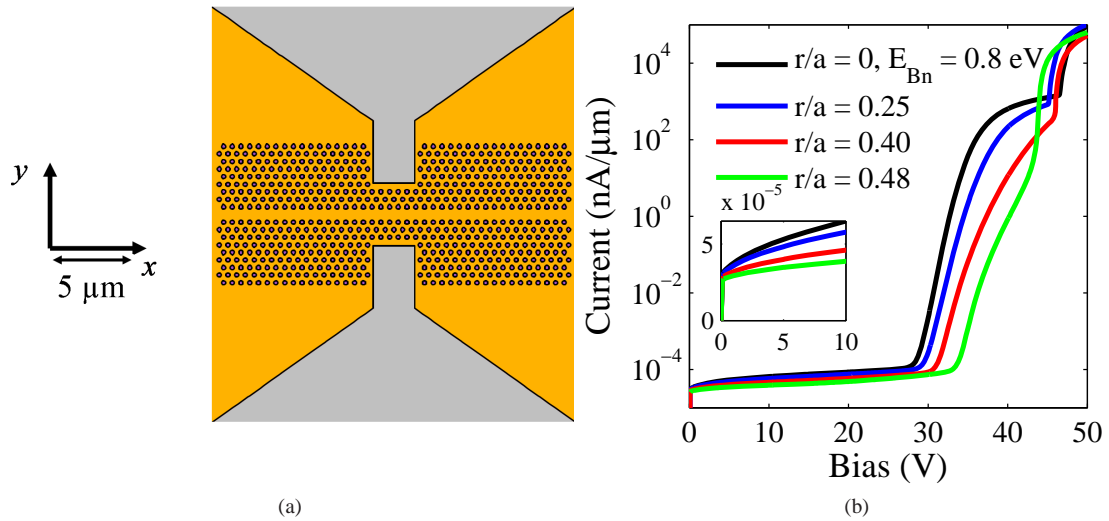


Fig. 2. (a) Simulated structure. The MSM junction (gray electrodes) is embedded near the cavity center (b) Semilog plot of current versus voltage for several radii of photonic crystal holes. Inset: zoom at low bias regime (linear plot)

while the second one above 40V is due to impact ionization. While this behavior is a common feature of MSM Schottky junctions [28], the comparison of the results for different radii of photonic crystal holes, from $r = 0$ to $r = 200$ nm, gives direct information on the impact of the photonic crystal itself. In the diffusion regime, the current is reduced approximately by the air-filling factor, similarly to what was reported in [15] [Fig. 2(b) inset]. Full depletion is reached at higher biases when the hole radius becomes larger, because the effective path through the structure becomes longer. Impact ionization becomes significant at lower biases in large radii structures, because the field can be very strong in the small silicon regions between the air holes. The main information here is that there is no drastic change in the $I(V)$ curve when the radius is 100 nm ($r/a = 0.25$), by comparison with the bulk case ($r = 0$). Therefore, we may believe that carrier collection is not impacted too much by the photonic crystal. As drift is a much faster collection mechanism than diffusion, we might expect that the carrier lifetime will be effectively reduced when full depletion of the interelectrode region is obtained (here at 30 V).

These conclusions were confirmed by simulations under illumination. We introduced a local carrier generation rate g proportional to the optical mode profile [Fig. 3(a)]. At null bias, the photogenerated carrier distribution [Fig. 3(b)] results from the convolution of the optical mode by the diffusion effects. A photocurrent circulates in the device [Fig. 3(c)] as soon as the bias is tuned. The effective lifetime is directly obtained from the carrier distribution and generation rate distribution as 330 ps. This lifetime is more than 10^3 smaller than the bulk SRH lifetime, because of diffusion out of the cavity and collection of the carriers that reach the small depleted region around the electrodes. Surface recombination at the Si-air interfaces is not taken into account here. When a polarisation is applied, the lifetime is reduced by a factor of 50, as the whole cavity gets depleted [Fig. 4]. The slight increase in the lifetime when $V > 30$ V is related to carrier multiplication by impact ionization. This means that the lifetime can get smaller than 10 ps. One can thus predict as shown in Fig. 1 that the effective quality factor of the cavity would not be influenced by FCA up to 1 mW input power. Furthermore most of the lifetime

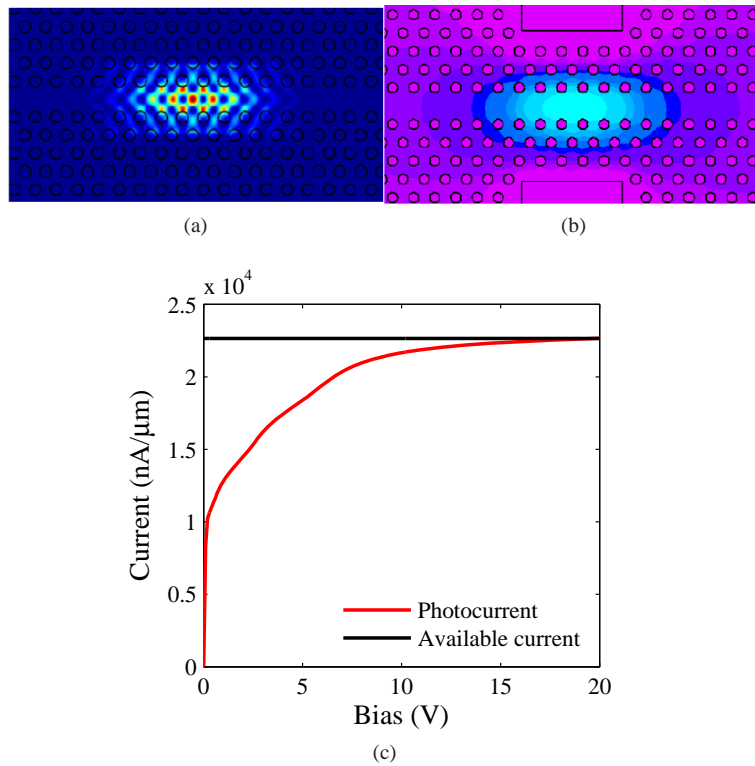


Fig. 3. (Simulation) (a) Optical mode profile of the width-modulated W1 waveguide photonic crystal cavity (b) Photogenerated carrier distribution ($V = 0$ V), resulting from the convolution of the optical mode profile by diffusion effects (c) Photocurrent vs. applied bias. The available current constant is the quantity one would obtain if all the generated carriers were collected. At 15 V, 99% of the carriers are collected.

reduction is attained at 20V, whereas the interelectrode region is not fully depleted yet. This is because carriers are generated essentially in the high optical energy region, near the cavity center. Only that region needs to be depleted in order to collect the carriers quickly.

In our design, for $V > 15V$, carriers have no time to recombine or to diffuse out of the depletion region before they are collected by the MSM junction. This can be checked by comparing the current circulating in the simulated electrodes with the available current one would have had if all the carriers were collected. The illumination current and the available current are plotted in Fig. 3(c). For $V > 15V$, all carriers are collected.

4. Experimental confirmation by EBIC measurements

The structures were fabricated from a silicon-on-insulator (SOI) substrate in two steps: first we fabricate the photonic crystal (electron beam lithography and dry etching), then platinum contacts are added, by electron-beam lithography followed by sputtering and lift-off. The quality of the contacts was checked by measuring the $I(V)$ characteristics. The results were similar in the bulk case and in the photonic crystal case, and is coherent with the simulated data. A typical example for a photonic crystal structure is given Fig. 5(a). The discontinuity at 23 V in the dark current curve is due to minority carrier current, meaning that the cavity is completely

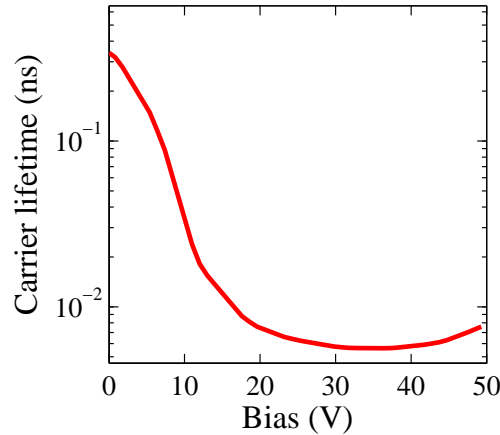


Fig. 4. (Simulation) Effective carrier lifetime depending on applied bias. The calculation is derived from the simulated carrier distribution. The lifetime is reduced 50 times at a 30 V bias.

depleted. Then the structure was optically probed by sweeping a continuous wave tunable laser from short to long wavelengths. The laser beam was laterally coupled into the sample through a lensed fiber, and propagated from the sample's edge to the photonic crystal through a silicon ridge waveguide. The optical output was collected and measured by a power meter. The coupling scheme is identical to that in [19].

We first tried to directly measure the expected increase of the effective quality factor when polarizing the junction. Indeed, applying a 20 V bias [Fig. 4] should (1) reduce the carrier lifetime to less than 20 ps and (2) remove the carriers introduced by residual impurities. The first effect impacts the effective quality factor that depends on the input power, as shown in Fig. 1. Effect (2) increases the intrinsic quality factor of the cavity by 4 % for $Q_0 = 50000$. Although at a high input power, effect (1) dominates because the photogenerated carrier density is larger than the residual impurity density, at a sufficiently low input power ($< 50 \mu\text{W}$), both effects should contribute significantly to the increase in the measured quality factor.

A typical example of two transmission spectra at $50 \mu\text{W}$, one at null bias and the other at high bias (20 V) is displayed on Fig. 5(b). The quality factor is extracted from the resonance width of the null bias spectrum as 36,600. The high bias spectrum is narrower. It is also red shifted and slightly asymmetrical. This effect is not due to thermal heating by the intra-band relaxation originating from FCA but is related to Joule heating: when the cavity is optically excited on resonance and the electrical bias is applied, a current of approximately $1 \mu\text{A}$ can flow in the junction resulting in several microwatts of dissipated electrical power near the PhC cavity center. As the wavelength approaches the resonance, there is more photocurrent, inducing a heating of the cavity by the Joule effect and a change in the refractive index, leading to a progressive shift of the resonant wavelength towards the longer wavelengths. This effect corresponds to a very small shift (5 pm) and temperature increase (0.001°C), but we cannot deduce the quality factor from the spectrum width anymore. Instead, we can consider the peak transmission Tr which does not change with the refractive index, and follows the relation $Q_{\text{eff}}/Q = (\text{Tr}/\text{Tr}_0)^{1/2}$. The increase in the peak transmission with the bias indicates a corresponding increase in the effective quality factor, from 36,600 to 38,300. This is good agreement with the values extracted from Eq. (2): for a null bias carrier lifetime and residual density taken as 0.6 ns and $6 \times 10^{15} \text{cm}^{-3}$, the quality factor increases from 36,600 to 38,300 when the carrier lifetime and

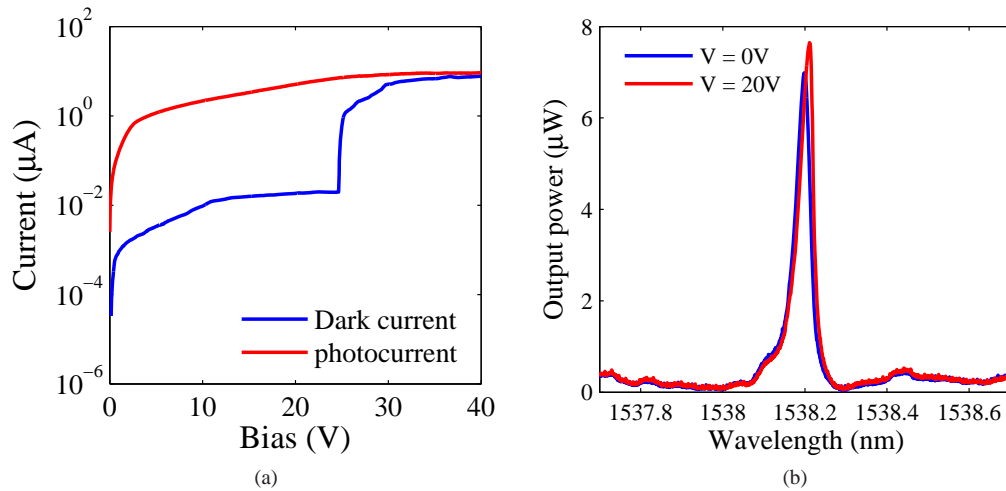


Fig. 5. (a) Dark current and photocurrent (surface illumination at visible wavelength in a Pt-Si-Pt photonic crystal junction. (b) Transmission spectra at 0 and 20 V, for $P_{in} = 50 \mu\text{W}$. The higher peak resonance at 20 V is attributed to a slight increase in the quality factor due to the removal of the free carriers and the reduction of free carrier lifetime. The red shift is due to Joule effect.

the residual carrier density go down to zero. The increase in peak transmission is thus almost certainly related to carrier depletion. In order to observe a larger effect, the input power was increased. As usual in silicon high quality factor resonators, continuous excitation at high power leads to thermal non-linear bistability and self-pulsating, and a straightforward interpretation of the spectra is not possible anymore. Time domain techniques would provide a more direct interpretation of the carrier dynamics. However, a pump-probe technique would be prone to sensitivity issues because the probe power must be kept low enough. Moreover, the time resolution may be poor when the carrier lifetime becomes of the same order as the photon lifetime in the cavity (50 ps). Resorting to an off-plane excitation of carriers (e.g. with a He:Ne laser) and still using a cw probe would allow the measurement of an undistorted Lorentzian lineshape, however the device would be operated under substantially different conditions.

The reduction of carrier lifetime is directly linked to the carrier depletion. What is really needed is to be sure that depletion does take place in the photonic crystal cavity. To get such evidence, we used Electron Beam Induced Current measurements (EBIC). EBIC [29–31] is a spatially resolved semiconductor analysis technique for examining carrier transport properties. As the electron beam of a Scanning Electron Microscope scans over the photonic crystal, the minority charge carriers which are generated in the depletion region are collected by the junction and contribute to the EBIC signal. In our set-up, the external amplifier circuit is contacted to the Pt electrodes directly in the SEM chamber, using tungsten probes driven by nanomanipulators. EBIC images taken at 1, 15, and 25 V are displayed in Figs. 6(a)–6(c), where one can see the bias induced enlargement of the depletion region. This proves the depletion extension by polarisation of a MSM junction is effective in a photonic crystal. A comparison with the simulated electron density concentration at the same three biases is provided by Figs. 6(d)–6(f). The shape of the simulated depletion regions are strikingly similar to the EBIC maps. This means that the 2D simulation model we undertook does capture the essential physics, even without taking into account surface recombination or level pinning at the air interface.

The existence of a non zero signal in the photonic crystal holes is attributed to carrier generation by secondary electrons induced by the excitation beam, and indicates that the EBIC pictures are noisy. Although, it is possible to extract some quantitative information: the size of the depletion region can be estimated as the distance between the electrode and the closest point beyond which the induced current variation is due only to the background noise. Therefore the estimated boundary between depletion and intrinsic region is located where the photonic crystal pattern becomes invisible. At 1, 15 and 25 V the depletion region sizes are estimated as 400 nm, 1.84 μm and 2.25 μm respectively, which is in very good agreement with the square root law given by Eq. (6) for $E_{Bn} = 0.84\text{eV}$ and $N_D = 6 \times 10^{15}\text{cm}^{-3}$ [Fig. 7]. At 25 V, the depletion region crosses the W1 waveguide. Almost all the high optical energy zone is depleted, and the remaining is very close ($< 0.5\mu\text{m}$) from the depletion region. Therefore, we can expect the effective carrier lifetime to be under 15ps, and to reduce by almost two the degradation of the quality factor at a 2 mW power (see Fig. 1). At the best of our knowledge, these kind of EBIC images are original in photonic crystal literature. They are particularly important as they confirm the validity of our simulation results and photonic crystal microcavity depletion design.

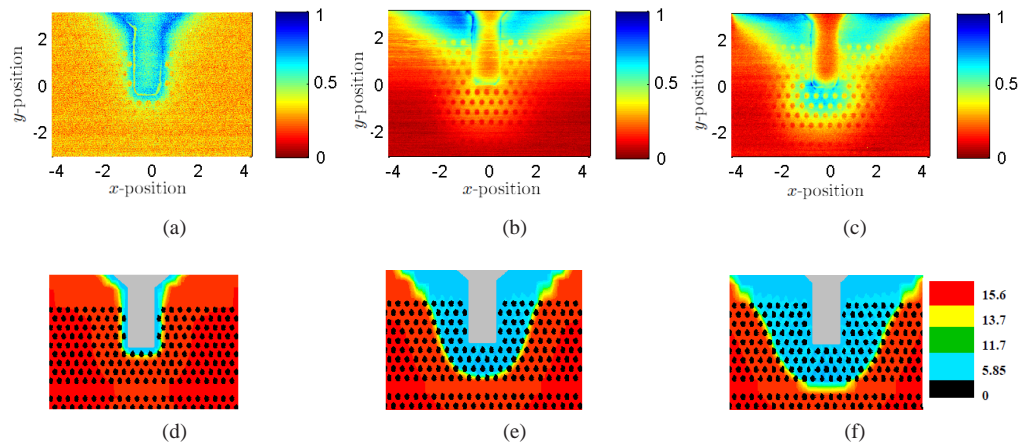


Fig. 6. Comparison of EBIC images at the cathode with simulated electron density (a)-(c) Normalised EBIC images of Pt-Si-Pt MSM junction on photonic crystal for different bias voltages under the following SEM conditions: High Voltage = 15 kV, probe current = 10 pA. In image (a), because of the low bias condition, the contribution of noise is much higher than in images (b) and (c). Therefore the contrast between depleted and intrinsic regions is smaller. (d)-(f) Simulated electron density, for the same three bias voltages. The colorbar unit is cm^{-3} (log scale) (a),(d): 1 V. (b),(e): 15 V. (c),(f): 25 V.

Further improvement of the design will be aimed at reducing the energy cost for having full depletion. In steady state, there is a Joule power dissipation proportional to the dark current and applied bias. To reduce the dark current, we chose to work in the diffusion regime ($V < V_{FB}$) and to use a high contact barrier metal (Platinum). The typical dark current in our sample is around 10 nA at 20 V. To work in the full-depletion regime and still have a low dark current, we could use an asymmetrical junction [32,33] such as Platinum-Si-Chrome. The chrome potential barrier will strongly limit the hole current. Finally, a passivation layer under the metal contacts outside the active region will reduce the dark current by a numerical factor. There are two means of reducing the voltage that is necessary to deplete the high energy mode region: to work with a purer sample and to bring the electrodes closer. In the second case, the optical design has to

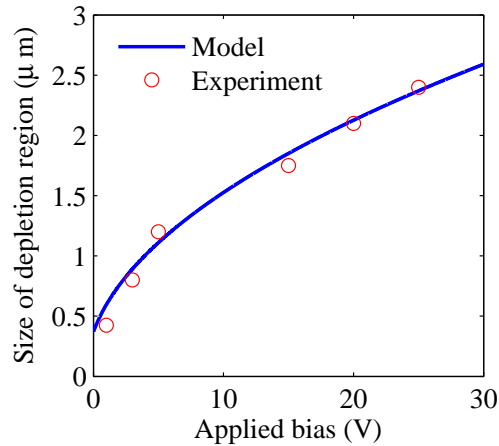


Fig. 7. Comparison of calculated depletion width (solid line) from Eq. (6) ($N_D = 6 \times 10^{15} \text{ cm}^{-3}$) and width extracted from EBIC images.

be adapted and the mode extension in the electrode direction shortened in order not to threaten the quality factor. If the impurity concentration is reduced to $N_D = 10^{15} \text{ cm}^{-3}$ and a 1.5 V bias is applied to the electrodes then, according to Eq. (6) with $E_{Bn} = 0.8 \text{ eV}$, $\epsilon_r = 11.9$, a 1.7- μm wide depletion region will be created. If the electrode spacing is 1.5 μm this means that full-depletion is reached at a bias below 1.5 V, which is a reasonable value for integrated silicon optical devices on CMOS-compatible chips. Overall, the Joule power consumption due to dark current in steady state could be smaller than 3 nW. All these improvements will also reduce the temperature increase created by Joule effect through dark current and photocurrent. Under strong optical injection however, heat is mainly generated by free carrier absorption. Therefore, when we remove the free carriers, even when taking into account the Joule effect, overall we do not heat up the cavity.

5. Conclusion

Metal deposition of microelectrodes on intrinsic silicon is a simple yet effective way of making a junction around a photonic crystal resonator. It can be designed so that the quality factor is preserved, and the dark current very low. We demonstrated that a MSM junction around a photonic crystal is a good candidate to reduce the undesirable effects of FCA in silicon non-linear devices. Effective carrier lifetimes down to 6 ps are predicted. A detailed numerical study and EBIC characterization of the fabricated structure show the spatial evolution of the depletion region. With a proper design, depletion of the high optical energy could be obtained at a small energy cost. Interesting applications of our simple architecture include the reduction of the threshold in Raman Si microlasers.

Acknowledgments

This work was supported by RTRA Triangle de la Physique through the DESIRABLE project and by Agence Nationale de la Recherche (ANR) through PHLORA project (ANR-2010-JCJC-0304 01). This work was also supported by the french RENATECH network and Conseil général de l'Essonne.